

The impact of reactive oxygen species coupled with moisture on bitumen long-term aging

Khalighi, Sadaf; Primerano, Kristina; Mirwald, Johannes; Hofko, Bernhard; Varveri, Aikaterini

DOI

[10.1080/14680629.2024.2438343](https://doi.org/10.1080/14680629.2024.2438343)

Publication date

2025

Document Version

Final published version

Published in

Road Materials and Pavement Design

Citation (APA)

Khalighi, S., Primerano, K., Mirwald, J., Hofko, B., & Varveri, A. (2025). The impact of reactive oxygen species coupled with moisture on bitumen long-term aging. *Road Materials and Pavement Design*, Article 2438343. <https://doi.org/10.1080/14680629.2024.2438343>

Important note

To cite this publication, please use the final published version (if applicable).
Please check the document version above.

Copyright

Other than for strictly personal use, it is not permitted to download, forward or distribute the text or part of it, without the consent of the author(s) and/or copyright holder(s), unless the work is under an open content license such as Creative Commons.

Takedown policy

Please contact us and provide details if you believe this document breaches copyrights.
We will remove access to the work immediately and investigate your claim.

Green Open Access added to TU Delft Institutional Repository





'You share, we take care!' - Taverne project

<https://www.openaccess.nl/en/you-share-we-take-care>

Otherwise as indicated in the copyright section: the publisher is the copyright holder of this work and the author uses the Dutch legislation to make this work public.



The impact of reactive oxygen species coupled with moisture on bitumen long-term aging

Sadaf Khalighi^a, Kristina Primerano ^b, Johannes Mirwald ^b, Bernhard Hofko ^b and Aikaterini Varveri ^a

^aDelft University of Technology, Delft, Netherlands; ^bChristian Doppler Laboratory for Chemo-Mechanical Analysis of Bituminous Materials, Institute of Transportation, TU Wien, Wien, Austria

ABSTRACT

Bitumen, a crucial constituent in the composition of asphalt pavements, plays a vital role in the performance and durability of pavements. Bitumen undergoes aging over time due to complex interactions between its chemical components and various environmental factors. In this investigation, the study focuses on examining the aging process of bitumen under the combined influence of moisture and reactive oxygen species (ROS). The findings highlight the importance of considering ROS and moisture as critical factors contributing to accelerated aging. Results obtained from Fourier-transform infrared (FTIR) spectroscopy, SARA fractionation, and optical inverse microscope (OIM), as well as dynamic shear rheometer (DSR) examination, indicate that the concurrent influence of these factors induces significant aging in bitumen, with the extent of this impact being modulated by the bitumen's inherent aging susceptibility. The insights obtained from this study enhance strategies to justify the destructive impacts of aging, extending the operational lifespan of asphalt pavements.

ARTICLE HISTORY

Received 13 March 2024
Accepted 1 December 2024

KEYWORDS

Viennese binder aging; moisture aging; FTIR; SARA fractionation; optical inverse microscopy; dynamic shear rheometer

Introduction

Bitumen, derived as a viscoelastic substance from the residual components of crude oil through refinery processes, serves a pivotal role as a binding agent in construction applications, notably in road and airfield pavements (Hofer et al., 2023; Read & Whiteoak, 2003). Due to its hydrocarbon nature, bitumen is susceptible to environmental aging factors. This degradation occurs in two distinct phases: short-term aging (STA) during mixture production, mixing, transportation, and pavement construction, and long-term aging (LTA) throughout its service life (Petersen, 2009). Processes such as the loss of volatiles, steric hindrance, and oxidation contribute to the asphalt binder's aging during these phases (Petersen, 2009). Oxidative aging, particularly, holds significance as it adversely affects pavement performance (Pipintakos et al., 2021). To effectively characterise bitumen and implement preventive and restorative measures, it is imperative to employ robust laboratory aging protocols (Hofer et al., 2023).

Established aging protocols at the binder level, such as the Rolling Thin Film Oven Test (RTFOT) and Pressure Aging Vessel (PAV) methods, are commonly employed (Hofko & Hospodka, 2016; Koyun et al., 2022; Nagabhushanarao & Vijayakumar, 2021). RTFOT involves subjecting binder films to a controlled airflow at 163°C for 75 min for short-term aging (STA) (EN 12607-1, 2014), while PAV for long-term aging (LTA) includes aging of bitumen films in a pressurised vessel with air at 2.07 MPa and temperatures of 90–110°C for 20 h (EN 14769, 2012). However, numerous studies highlight limitations in accurately replicating field conditions and predicting natural pavement aging with these methods

(Petersen, 2009). Discrepancies between laboratory and field-aged samples are discussed in available literature sources (Airey, 2003; Besamusca et al., 2012; Erskine et al., 2012; Jing et al., 2019, 2020, 2021, 2022; Lu et al., 2008; Qian et al., 2020; Qin et al., 2014; Singhvi et al., 2022). These variations may result from the omission of environmental aging factors in laboratory protocols. Real-world conditions expose bitumen to various aging agents, including moisture, high concentrations of car emissions and reactive oxygen species (ROS), which are not considered in routine aging protocols. An ideal aging protocol should encompass all these factors and accelerate their effects to simulate field aging efficiently. Before incorporating these factors, understanding the individual effects is essential. This study specifically focuses on the impact of moisture and ROS on bitumen aging.

Numerous investigations have already documented the influence of moisture on the degradation process of bitumen and asphalt. Two main categories characterise the relevant studies: experimental investigations and molecular dynamic simulations. Ma et al. conducted a molecular dynamic simulation explaining the impact of hydrogen bonding interactions and water clustering at diverse temperature and water content conditions, influencing the self-diffusion coefficient of water. The density, glass transition temperature, viscosity, and cohesive energy for bitumen were computed. Generally, an increase in water content corresponds to a decrease in these parameters (Ma et al., 2023). Experimental findings emphasise the detrimental impact of moisture, coupled with mechanical stresses, leading to strength and durability reduction, causing binder and aggregate debonding, as well as adhesive or cohesive failure (Airey et al., 2008; Cong et al., 2021; Valentin et al., 2021; Valentová et al., 2016). Notably, Omar et al. underscored the significance of moisture infiltration in asphalt pavements, observing diminished adhesive performance between aggregate surfaces and bitumen due to water molecule diffusion (Omar et al., 2020). This decline in adhesive properties contributes to issues such as looseness, spalling, and potholes in the asphalt pavement. Khalighi et al. demonstrated that hygrothermal aging, involving both heat and moisture, accelerates the aging process more effectively than thermo-oxidative aging alone (Khalighi et al., 2024). Additionally, the interaction of bitumen with aqueous solutions containing salts (e.g. NaCl and Na₂SO₄) alters the surface roughness of asphalt mixtures and accelerates the erosion process, as highlighted by Zou et al. (Zou et al., 2021). Das et al. provided evidence of the formation of water-soluble thin films due to aging (Das et al., 2015), while Varveri et al. revealed the detrimental impact of moisture on the fracture characteristics of asphalt mortars, particularly in terms of low-temperature properties (Varveri, 2017). Despite some studies indicating minimal influence of water on bitumen and asphalt aging (López-Montero & Miró, 2016), or variations in the influence of moisture among different bitumen types (Huang et al., 2008), further research is necessary to explore the specific effects of water.

In addition to the impact of moisture on aging, the role of the atmosphere and the presence of reactive oxygen species (ROS) such as ozone (O₃) and nitrogen oxides (NO_x) is of immense importance. Ozone formation occurs in the atmosphere through the oxidation of hydrocarbons and carbon monoxide (CO) (Jacob, 2000), while NO_x is emitted from car engines (Singh et al., 2022), particularly near asphalt pavements within the traffic system. However, the available literature on the effects of realistic aging conditions, including ROS, on bitumen or related materials is scarce and widely scattered. To incorporate ROS in the aging process, Mirwald et al. developed the Viennese Binder Aging (VBA) method, in which samples are exposed to air enriched with a combination of ozone (O₃) and nitrogen oxides (NO_x) (Mirwald et al., 2020a). The elevated concentrations of these oxidant gases serve as the primary aging-inducing factors, while other parameters such as temperature and pressure are maintained as close to realistic conditions as possible. They showed that with VBA, a RTFOT + PAV level of aging is surpassed within three days at 80°C. Hofko et al. investigated the effect of O₃ solely and in combination with NO_x on bitumen recovered from aged asphalt specimens (Hofko et al., 2020). Their results reveal that significant aging occurred only in the presence of NO_x. This finding was further confirmed by Hofer et al., who exposed three different unmodified bitumen samples separately to NO, NO₂ and O₃ (Hofer et al., 2022). They observed that the effect of O₃ was mild compared to NO₂, which induced significant aging even at low concentrations, suggesting that NO₂ may function as an aging enhancer and/or accelerator in the presence of another oxygen source such as air. In another

study conducted by Hofer et al., multiple cycles of the Pressure Aging Vessel (PAV), Viennese Binder Aging (VBA) and field aging data were compared (Hofer et al., 2023). This study has demonstrated that the formation of ketones, indicated by the band at 1700 cm^{-1} , significantly increases with both aging methods, with the VBA method yielding a 110% increase compared to a 42% increase observed in the 1xPAV sample. This suggests that VBA may accelerate certain oxidative reactions more effectively than PAV. Additionally, analysis of aromatic structures reveals similar levels of aromaticity between the VBA and 5xPAV samples, indicating that both methods contribute comparably to structural changes in the binder. However, the presence of sulphurous oxidation products and their respective bands indicate that the NO_2 -aged samples exhibit characteristics more akin to field-aged samples, highlighting the complexity of chemical transformations during aging. Notably, the field-aged sample consistently shows the highest absorbance across all investigated bands, underscoring that neither laboratory method fully replicates the extensive aging experienced in real-world conditions. However, the VBA method provided a better approximation compared to the standard aging procedure, enabling a more accurate qualitative simulation of the chemical properties of the investigated field samples.

The aim of this research is to examine the impact of combined moisture and reactive oxygen species (ROS) aging on two unmodified binders from different crude oil sources. To achieve this objective, the unmodified bitumen, which had undergone short-term aging, was subjected to long-term aging through two different methods. Firstly, the Viennese Binder Aging (VBA) technique was employed, exposing the specimen to technically dry air enriched with nitrogen dioxide (NO_2) and ozone (O_3). Secondly, the sample underwent long-term aging using the same VBA protocol in conjunction with 75 g/m^3 absolute humidity. To characterise the aged binder samples, several analytical techniques were utilised, including Fourier-transform infrared (FTIR) spectroscopy, separation of asphaltenes, resins, aromatics, and saturates (SARA) fractionation using solid phase extraction (SPE) cartridges, and the application of an Optical Inverse Bright-field, Dark-field, Fluorescence Microscope (OIM), frequency sweep test and relaxation test.

Material and method

Material

In this study, Q 70/100 and T 70/100 unmodified binders were used to prepare films of 1 mm thickness in glass petri-dishes with 78.5 cm^2 surface area. Table 1 shows the main specification of the examined bitumen.

Sample preparation and aging conditions

Both Q 70/100 and T 70/100 bitumen samples were subjected to laboratory aging using a standardised approach. Specifically, a simulation of short-term aging (STA) was conducted by exposing 3.2 mm thick bitumen films to the Thin Film Oven Test (TFOT) at a temperature of 163°C for a duration of 5 h. TFOT was selected due to its reliability and ease of performance compared to RTFOT. This procedure

Table 1. Specifications of Q 70/100 and T 70/100 at fresh (unaged) state.

Property		Unit	Q PEN 70/100	T PEN 70/100
Penetration at 25°C		0.1 mm	70–100	70–100
Softening point		$^\circ\text{C}$	43–51	43–51
Complex shear modulus at 1.6 Hz & 60°C		kPa	1.8	2.3
Phase angle at 1.6 Hz & 60°C		$^\circ$	88	88
Chemicals	Nitrogen N	(%)	0.59	0.93
	Carbon C		79.19	87.23
	Hydrogen H		10.81	11.26
	Sulphur S		4.47	3.35
	Oxygen O		2.25	0.60

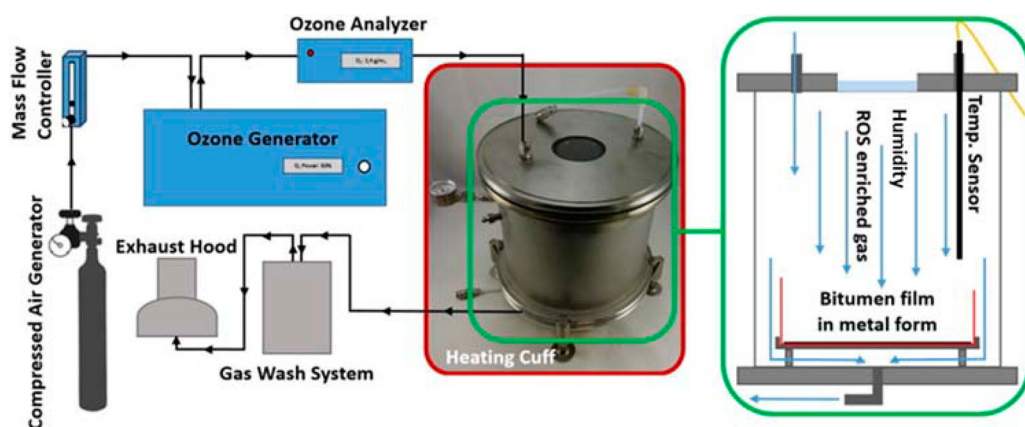


Figure 1. Scheme of the VBA aging setup (Mirwald et al., 2020a).

was performed in accordance with the EN 12607-2 test standard (EN 12607-2, 2014). To ensure consistent film thickness, the corresponding weights of bitumen were calculated based on the available surface areas (78.5 cm^2) of petri dishes and the density of bitumen. These calculated weights were then added to each petri dish, resulting in films with a thickness of 1 mm. The petri dishes were subsequently placed in an oven at 160°C for 5 min to obtain flat films. The films were allowed to cool at room temperature (25°C) for a period of two hours prior to undergoing long-term aging.

For the simulation of long-term aging (LTA), Viennese binder aging (VBA) was employed. This method was introduced by Mirwald et al. (2020a) as a means of replicating long-term aging of bitumen (Mirwald et al., 2020a). In this approach, an elevated concentration of reactive oxygen species (ROS) in the form of O_3 and NO_x was utilised as the primary factor inducing aging. In this study, an aging atmosphere consisting of air enriched with 25 parts per million (ppm) of NO_2 and 4 gr/m^3 of ozone was chosen based on previous optimisation of these parameters in reference (Hofer et al., 2023). The selection of this specific aging atmosphere was based on the high oxidation potential of NO_2 in air when it comes to bitumen. The mixture of NO_2 and ozone was directly introduced at the inlet of the aging cell. Detailed information regarding the aging setup employed in this study can be found in the publication by Hofer et al. (2023). The experiment was conducted at a controlled temperature of $85 \pm 1^\circ\text{C}$, with a total aging duration of three days. This method is called 'VBA-Dry' in the rest of this text. This technically dry condition had 5 g/m^3 absolute humidity which is equal to 1.5% relative humidity at 85°C . To introduce moisture in the aging protocol, water spray was used to create 75 g/m^3 absolute humidity (21% relative humidity at 85°C) in the VBA chamber (Figure 1). This humidity level was chosen to prevent any harm to the aging chamber. The humidity was created by spraying water for 0.1 s with 105-s intervals at a pressure of 1.6 bar in both the water tank and air nozzle. The same concentration of oxidative gases was applied as the VBA-Dry. The combination of VBA and water spray is named 'VBA-Wet' in this work. For control groups in this study, oven aging at 85°C was conducted under both dry conditions (named as 'Oven') and conditions with humidity (75 g/m^3 absolute humidity or 21% relative humidity) (named as '21%RH') for three days.

Fourier-transformation infrared (FTIR) spectroscopy

ATR-FTIR spectroscopy serves as a valuable tool for acquiring insights into the chemical composition of the analysed sample, particularly as it undergoes specific transformations during the aging process. To prepare the samples, approximately 1 g of the material was meticulously heated in a metal spoon above a heat gun until it reached a temperature of 110°C . Subsequently, stirring was performed for

Table 2. Main functional groups of bitumen in FTIR spectra (Hofer et al., 2023; Jing et al., 2018).

Area	Vertical band limit (cm ⁻¹)	Functional groups
A ₈₁₀	710–912	Hydrocarbon chain, (CH ₂) _n and CH
A ₁₀₃₀	1047–995	Oxygenated function-sulphoxide, S = O
A ₁₂₀₀	1200–1350	Tertiary alcohol C–O, C–O in carboxylic acid, C–C–C in diaryl ketones, C–N secondary amides, O = S = O in sulphone
A ₁₃₇₆	1390–1350	Branched aliphatic structures, CH ₃
A ₁₄₆₀	1525–1395	Aliphatic structures, CH ₃ and CH ₂
A ₁₆₀₀	1670–1535	Aromatic structure, C = C
A ₁₇₀₀	1753–1685	Oxygenated function-carbonyl, C = O
A ₂₉₅₃	2990–2880	Aliphatic structures, Symmetric, Asymmetric stretching, CH ₃
A ₃₃₀₀	3100–3600	Hydroxyl structure, OH

a duration of 3 min using the tip of a thermometer. Small droplets of the material were then carefully transferred onto a silicon foil and covered with a lid to prevent contamination from dust or light-induced aging on the surface of the binder. In the process of sample preparation, the general recommendations put forth by Mirwald et al. (2020a, 2020b) were taken into careful consideration. The measurements were conducted using a Bruker Alpha II instrument, equipped with a deuterated triglycine sulphate (DTGS) detector and an attenuated total reflection unit featuring a diamond crystal. Each spectrum was generated by collecting data from 24 scans, employing a resolution of 4 cm⁻¹. Three spectra were acquired for each droplet in the range of 4000–400 cm⁻¹. For each aging state, a total of three samples were prepared and analysed in the solid state, resulting in nine spectra per aging state.

To quantify the specific functional groups of interest, including carbonyl, sulphoxide, sulphone, aliphatic, long chain, aromaticity, and hydroxyl groups, indices were determined based on predefined wavenumber ranges. The calculation of these indices involved employing equations designated for each functional group (equations (1)–(8)), with the vertical limits specified in Table 2. Prior to the calculation of the indices, the spectra underwent appropriate normalisation and baseline corrections. The areas to the baseline and the total area of the spectra were utilised as references in the computation of aging indices.

$$\text{Sulfoxide index} = A_{1030} / A_{\text{total}} \quad (1)$$

$$\text{Sulfone index} = A_{1200} / A_{\text{total}} \quad (2)$$

$$\text{Aromaticity index} = A_{1600} / A_{\text{total}} \quad (3)$$

$$\text{Long chain index} = A_{810} / A_{\text{total}} \quad (4)$$

$$\text{Aliphatic index} = A_{1376} + A_{1460} + A_{2953} / A_{\text{total}} \quad (5)$$

$$\text{Carbonyl index} = A_{1700} / A_{\text{total}} \quad (6)$$

$$\text{Hydroxyl index} = A_{3300} / A_{\text{total}} \quad (7)$$

$$A_{\text{total}} = A_{810} + A_{1030} + A_{1200} + A_{1376} + A_{1460} + A_{1600} + A_{1700} + A_{2953} + A_{3300} \quad (8)$$

Frequency sweep

The evaluation of the Complex shear modulus (G^*) and phase angle (δ) was performed using a dynamic shear rheometer (DSR) under oscillatory loading conditions. This involved the measurement of these rheological properties across various temperatures and frequencies. The DSR tests were conducted using an 8 mm diameter parallel plate with a 2 mm gap. The temperature range for testing spanned from 0 to 40°C in 10°C increments. Likewise, the frequency range extended from 10 to 0.1 Hz, equivalent to 62.8 to 0.628 rad/s, while maintaining a consistent strain load of 0.1% (Jing et al., 2020). To facilitate analysis and enable comparisons, master curves for the complex modulus and phase angle

were constructed using the time-temperature superposition principle (TTSP), with a reference temperature set at 20°C. Each measurement strictly adhered to standard testing protocols (AASHTO T 315-19 (T315, 2012)), and to ensure data consistency, duplicate testing was performed for each sample.

Relaxation

Stress relaxation is a vital property of bitumen, indicating its ability to dissipate stress under constant strain conditions. To assess stress relaxation, a test was conducted using a DSR with an 8-mm-diameter parallel plate and a 2 mm gap. The examination was conducted at a temperature of 0°C, utilising a strain-controlled mode. Initially, the strain was incremented from 0 to 1% shear strain within 0.1 s. Following this, the shear strain was sustained at 1% for a duration of 100 s, during which alterations in shear stress were recorded to assess the material's relaxation behaviour (Jing et al., 2020).

SARA fractionation

The bitumen samples after each stage of aging were subjected to fractionation into saturates, aromatics, resins and asphaltenes using a solid phase extraction (SPE) fractionation method, as described by Sakib and Bhasin (Sakib & Bhasin, 2019). Approximately 400 ± 20 mg of the respective sample was stirred for 24 ± 2 h in 40 ml of n-heptane, resulting in a solution of maltenes and a residue of insoluble asphaltenes in n-heptane. To separate these two fractions, Thermo Scientific™ Titan3™ PTFE syringe filters with a diameter of 25 mm and a pore size of 0.2 μm were utilised. These filters were mounted on four syringes, each filled with 10 ml of the maltene/asphaltene mixture. The solution was gently pulled through the filters using a vacuum pump and collected in 40 ml glass vials. Subsequently, each filter was washed with an additional 5 ml of n-heptane to ensure the collection of any remaining maltenes.

Of the resulting four maltene solutions (15 ml each), two were dried under a continuous stream of nitrogen gas at approximately 120°C, and the remaining residue was weighed. The other two solutions were diluted to a maltene concentration of 3.33 mg/ml and applied to Thermo Scientific™ HyperSep™ Silica SPE cartridges with a pore size of 40–63 μm . Different solvents were employed to elute the saturates, aromatics, and resins fractions. For the saturates, 10 ml of n-heptane was used, whereas for the aromatics, 25 ml of an 80% toluene – 20% n-heptane mixture (v/v) was utilised. As for the resins, 40 ml of a 90% dichloromethane – 10% methanol mixture (v/v) was employed. The obtained solutions were once again dried under a continuous stream of nitrogen gas at approximately 120°C, and the mass of each fraction was determined gravimetrically. This separation procedure was repeated for two samples per binder.

By measuring the SARA fractions, the colloidal index (CI) of the samples can be calculated. The CI is a ratio of the sum of quantities of resins and aromatics to the sum of quantities of saturates and asphaltenes. This ratio can be used to estimate the stability of the crude oil with respect to asphaltenes. The CI is calculated as per equation (9):

$$\text{CI} = \frac{\text{Resins} + \text{Aromatics}}{\text{Asphaltenes} + \text{Saturates}} \quad (9)$$

The polarity ratio, i.e. the ratio of highly polar (resin and asphaltenes) to light molecular weight (saturated and aromatic) fractions, is calculated as followed by equation (10):

$$\text{Polarity ratio} = \frac{\text{Resins} + \text{Asphaltenes}}{\text{Aromatics} + \text{Saturates}} \quad (10)$$

Optical inverse bright-, darkfield and fluorescence microscope (OIM)

One of the microscopic setups employed in capturing the microstructures of the binders was a Nikon Optical Inverse bright-, darkfield and fluorescence microscope (OIM). A schematic drawing illustrating the distinctions in the working modes can be found in the publication by Mirwald et al. (2022b).

The microscope setup entails of an industrial flexible column stand, a motorised Märzhäuser stage (X, Y, Z), a 100x CFI TU Plan objective (BD 100x, N.A. 0.80, W.D. 4.5 mm), a Nikon DS-Fi3 camera, an epi fluorescence unit and a pE-4000-Universal LED serving as the light source. The pE-4000-Universal LED comprises 15 different LEDs ranging from 365 to 770 nm. For bright- and dark-field imaging, the 500 nm LED was selected to minimise the potential impact on oxidation reactions while still maintaining an adequate contrast-to-illumination ratio (Mirwald et al., 2022b). The epi unit encompasses three different filter blocks for bright-field, dark-field and fluorescence, respectively. The exposure time for bright-field images was set at 5 ms, whereas dark-field images were captured with an exposure time of 900 ms. The discrepancy in exposure time can be attributed to the divergent underlying principles of the two modes. The bright-field filter block and objective do not impede any light from the light source, whereas the dark-field filter block and objective obstruct light in the centre of the illumination cone, allowing only light from the outer region to reach the sample surface at a 45° angle. If there is no light scattering from the surface or subsurface of the material, the camera does not capture any information, resulting in a dark image. However, if there are light-scattering particles near the surface of the sample, the incident light undergoes scattering and alters its angle of reflection. This scattered light with a modified angle of reflection passes through a dichroic mirror and is detected by the camera. As the overall intensity of light in dark-field imaging is significantly lower than in bright-field, a longer illumination time is required to achieve adequate contrast. A custom-made filter comprising an excitation filter at 403/95 nm (353–452 nm), an emission filter (long pass) at 500 nm, and a dichroic mirror at 495 nm was employed for fluorescence mode. Considering that the fluorescence of the bitumen is much weaker than the reflection observed in bright-field mode, an exposure time of 500 ms was selected. All images were acquired using the NIS elements BR software. Due to the non-planar nature of the sample surfaces, a z-stacking tool was utilised to capture images within a range of $\pm 10 \mu\text{m}$ around the focal plane of the binder specimen, followed by subsequent merging of the z-stacked images to generate a focused image. The resulting bright-field, dark-field and fluorescence images are directly presented in the results section. Furthermore, the dark-field images are employed for particle analysis, which will be discussed in the subsequent subsection. A total of 3 images per mode (bright-field or fluorescence) and binder were recorded. Since dark-field microscopy is utilised for quantification, three different spots per sample were recorded, resulting in nine dark-field images per binder, which are later used for particle analysis (Mirwald et al., 2022a).

Result and discussion

Fourier-transformation infrared (FTIR) spectroscopy

FTIR spectroscopy was performed to obtain information about chemical functional groups in bitumen samples. Figure 2a and b show a set of representative spectra obtained for Q and T bitumen, respectively. With this information it is possible to compare the degree of aging of the samples. To achieve this goal, seven different functional groups were analysed. The most used indices for aging studies are sulfoxide and carbonyl indices. Figure 3 shows that both the carbonyl and sulfoxide indices increased after short- and long-term aging. In the comparison between oven-aged samples and samples aged solely with humidity, a similarity in carbonyl and sulfoxide indices is obvious. Notably, the samples subjected to oven aging display elevated concentrations of sulfoxide and carbonyl products for T and Q samples, respectively. The observed variation can be attributed to the distinct sensitivity of binders, influencing the production of diverse functional groups during the aging process. Additionally, the reduced availability of oxygen within chambers maintained at 21% humidity contributes to this phenomenon. Interestingly, aging with a combination of ROS, high temperature, and moisture resulted in harsher aging conditions compared to aging using each individually. An explanation for this observation could be the reaction between reactive species in ROS and water vapour molecules, which may generate more oxidative species in the aging chamber. The effect of VBA-Wet aging strongly depends on the aging sensitivity of each bitumen. T bitumen showed a dramatic difference in indices

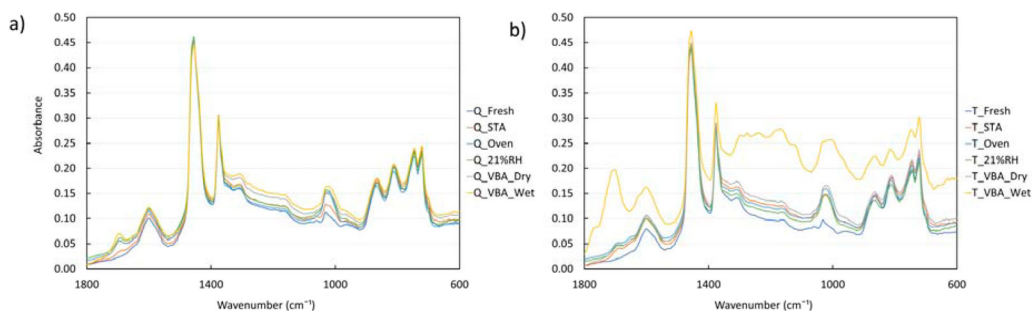


Figure 2. FTIR spectra of (a) Q and (b) T binder in different aging states, i.e. fresh, short-term aged, oven aged, humidity aged, VBA-Dry and VBA-Wet.

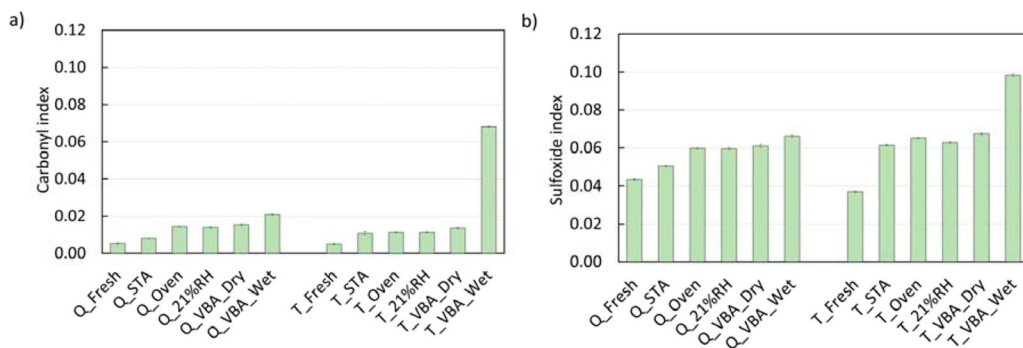


Figure 3. FTIR results for Q and T binders, (a) carbonyl, (b) sulphoxide.

between VBA-Wet and VBA-Dry, while the Q sample showed a moderate increase from the VBA-Dry to the VBA-Wet condition. Hence, it is concluded that the T sample exhibits greater sensitivity to coupled aging conditions. Given that aging with only humidity did not alter the aging level of the binders more than oven aging, it suggests that this binder is particularly responsive to conditions where ROS and humidity are combined.

In addition to the carbonyl and sulfoxide indices, hydroxyl, aromatic, sulphone, long-chain and aliphatic indices were studied to closely follow the aging mechanism, see Figure 4. The hydroxyl index remained relatively constant after ageing for both the long-term aged Q and T samples. This observation suggests that the formation of alcohols (indicated by the hydroxyl index) was not part of the aging reaction of the bitumen in this experiment. In addition, the indices for aromatics and sulphones increased after both short-term and long-term aging. The oxidation processes in the binders lead to an increase in aromaticity, which explains a higher value of the aromatics index after aging (Mirwald et al., 2020b). Interestingly, the VBA-Wet samples showed the highest value of aromaticity index, indicating that binders are more sensitive to aging in the simultaneous presence of ROS and water vapour. The sulphone region represents different oxidation products and usually shows a shift to higher absorption with aging, which can be explained by an increase in highly polar structures and thus the overall polarity of the material studied. However, the visible bands between 1350 and 1100 cm^{-1} could also be attributed to several other functional groups, such as methylene and aromatic group deformation vibrations ($=\text{C}-\text{H}$ in-plane), or skeletal vibrations of branched aliphatic motifs. Other possible contributors to this region include tertiary alcohols ($\text{C}-\text{C}-\text{O}$), carboxylic acids ($\text{C}-\text{O}$), diaryl ketones ($\text{C}-\text{C}-\text{C}$), secondary amides ($\text{C}-\text{N}$) and sulphone ($\text{O}=\text{S}=\text{O}$). A precise and unambiguous assignment of these bands remains challenging due to the overlap of signals from different functional groups. The deconvolution of FTIR spectra may serve as a potential approach to understand the overlapping peaks

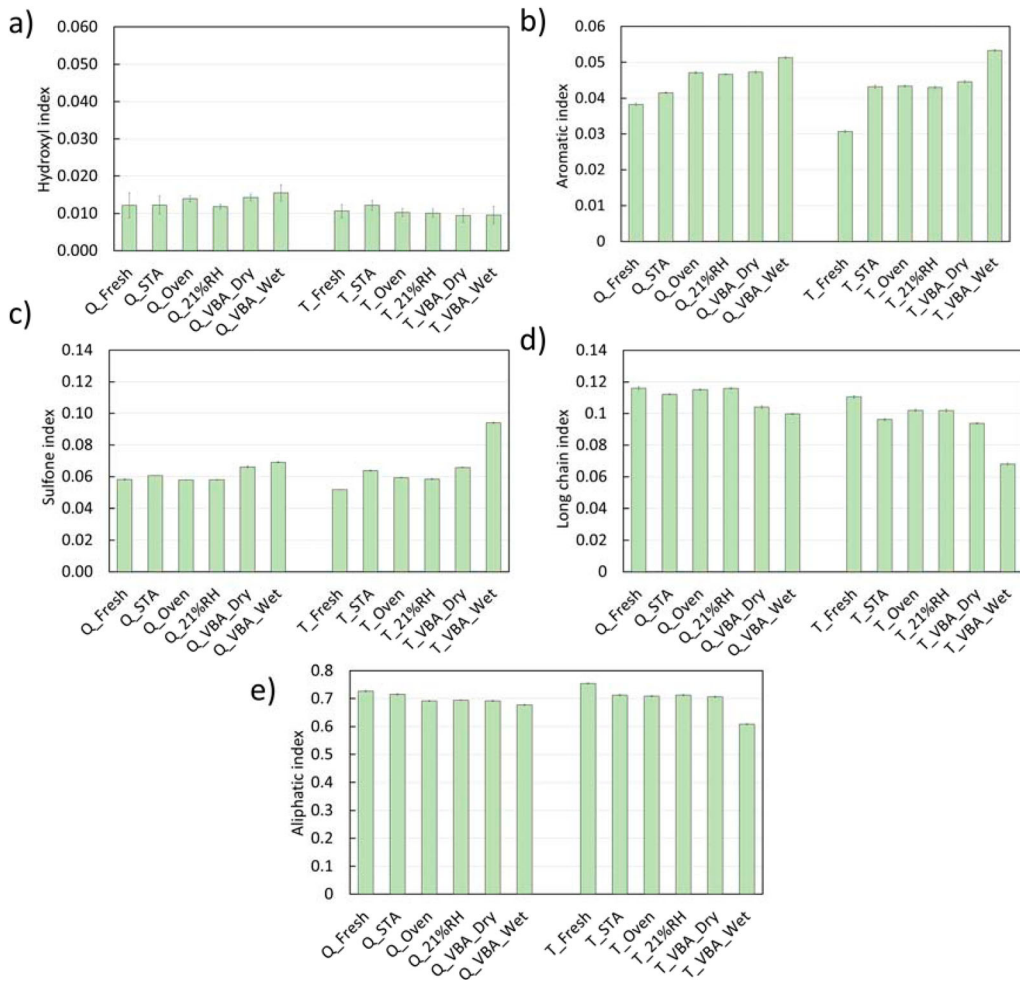


Figure 4. FTIR results for Q and T binders, (a) hydroxyl, (b) aromatic, (c) sulphone, (d) long chain, (e) aliphatic indices.

within this region. In relation to wet and dry aging conditions, our findings show that the aging process under VBA-WET condition significantly increased the intensity of this region compared to VBA-DRY condition. This suggests that the presence of humidity enhances the formation of polar structures, although the exact nature of these structures cannot be determined with certainty based on current spectral resolution. The elevated humidity in the VBA-WET setup appears to facilitate more intense oxidative processes, leading to a higher concentration of polar compounds. This observation is consistent with literature indicating that field oxidative aging in the presence of moisture can promote alcohol formation (Werkovits et al., 2023). Alcohol formation during aging is linked to the oxidation of branched aliphatic chains. The interaction of moisture with reactive oxygen species (ROS) may facilitate the formation of hydroxylated structures, including tertiary alcohols, likely through enhanced nucleophilic attack by water on electrophilic intermediates generated during oxidation. However, the precise mechanism of alcohol formation requires further investigation. The long-chain index in aged samples, whether subjected to short-term or long-term aging, demonstrated a decline in comparison to the fresh condition. Furthermore, the introduction of ROS and the simultaneous exposure to ROS and humidity further decreased the long chain index. For future studies, it would be helpful to divide different parts of the spectrum in long chain region into subgroups for further analysis. Finally,

the aliphatic index decreased after short- and long-term aging. Again, sample T-VBA-Wet showed the strongest decrease, i.e. the highest aging level.

A plausible explanation for the higher aging susceptibility of binder T lies in its elemental composition and structural characteristics. Binder T contains a higher carbon content (Table 1), and a higher C/H ratio (7.74) compared to binder Q (7.32), which suggests a higher proportion of C = C structures in binder T. These C = C structures are known to be less stable and more reactive, making them particularly susceptible to degradation under harsh aging conditions, such as those encountered during the VBA-Wet aging process. This increased reactivity leads to more pronounced changes in binder T during wet aging compared to binder Q.

Moreover, the higher initial stiffness of binder T (Table 1) indicates that its molecular structure is more rigid from the outset, which can make it more prone to embrittlement and degradation when subjected to aging processes. This is further supported by the lower oxygen content in binder T, indicating that it has undergone less oxidation initially and, therefore, has a greater potential for further aging compared to binder Q. As a result, binder T is more reactive and more likely to experience significant changes when exposed to aging conditions, particularly in the presence of moisture, leading to the observed differences between the wet and dry aging outcomes.

In summary, carbonyl, sulfoxide, aromatic and aliphatic indices can be useful for monitoring the degree of aging of bitumen. While long chain, sulphone and hydroxyl indices were not helpful to clearly identify the aging patterns and require more detailed studies. In general, the coupled aging of ROS and moisture is stronger for bitumen aging than only ROS.

Dynamic shear rheometer

Following short-term aging and long-term aging, the bitumen samples underwent assessment using the Dynamic Shear Rheometer (DSR), with two sample replicates for each condition. Utilising the Time-Temperature Superposition (TTS) principle, comprehensive master curves were meticulously constructed for both the complex shear modulus and phase angle, with a reference temperature of 20°C. Figure 5a and b depict the complex modulus and phase angle master curves of Q and T binders, respectively. For both binders, clear distinctions are observed between fresh, short-term aged, and long-term aged samples, with increased G^* values and decreased phase angle values due to aging. In the case of Q samples, a slight difference is evident in the phase angle master curves. Notably, at high and medium frequencies, the samples subjected to oven aging exhibit a slightly greater degree of aging compared to those aged solely with humidity. This correlation aligns with the FTIR results, wherein the carbonyl index of the oven-aged sample is marginally higher than that of the humidity-aged sample. Furthermore, there is an overlap observed between the VBA-Wet and VBA-Dry samples. This observation shows the low sensitivity of Q samples regarding the presence of humidity during aging.

In contrast, for T sample, the oven-aged samples and those aged exclusively with humidity exhibited overlap across the majority of the frequency range. However, divergence occurred at low frequencies, indicating increased aging for oven-aged samples. This finding is consistent with the observed change in the sulfoxide index, which also demonstrated more pronounced aging in oven-aged samples. The fluctuations observed in the phase angle master curve indicate an increased sensitivity of the phase angle concerning the aging conditions. Notably, for T samples, VBA-Wet exhibits a significant increase in G^* and a notable decrease in phase angle. These findings align with the results from FTIR analyses, indicating that VBA-Wet induces more substantial aging in T binder compared to Q binder.

Furthermore, during the analysis, two key parameters were computed: the crossover frequency (CR-Fr) and the crossover complex modulus (CR-CM). These metrics correspond to the frequency and complex modulus at which the phase angle reaches 45° and the storage modulus equals the loss modulus, respectively. They serve as valuable indicators of the transition in bitumen's viscoelastic behaviour, marking the shift from liquid-like to solid-like characteristics. Previous research has established a connection between lower CR-Fr values in aged bitumen and characteristics like higher

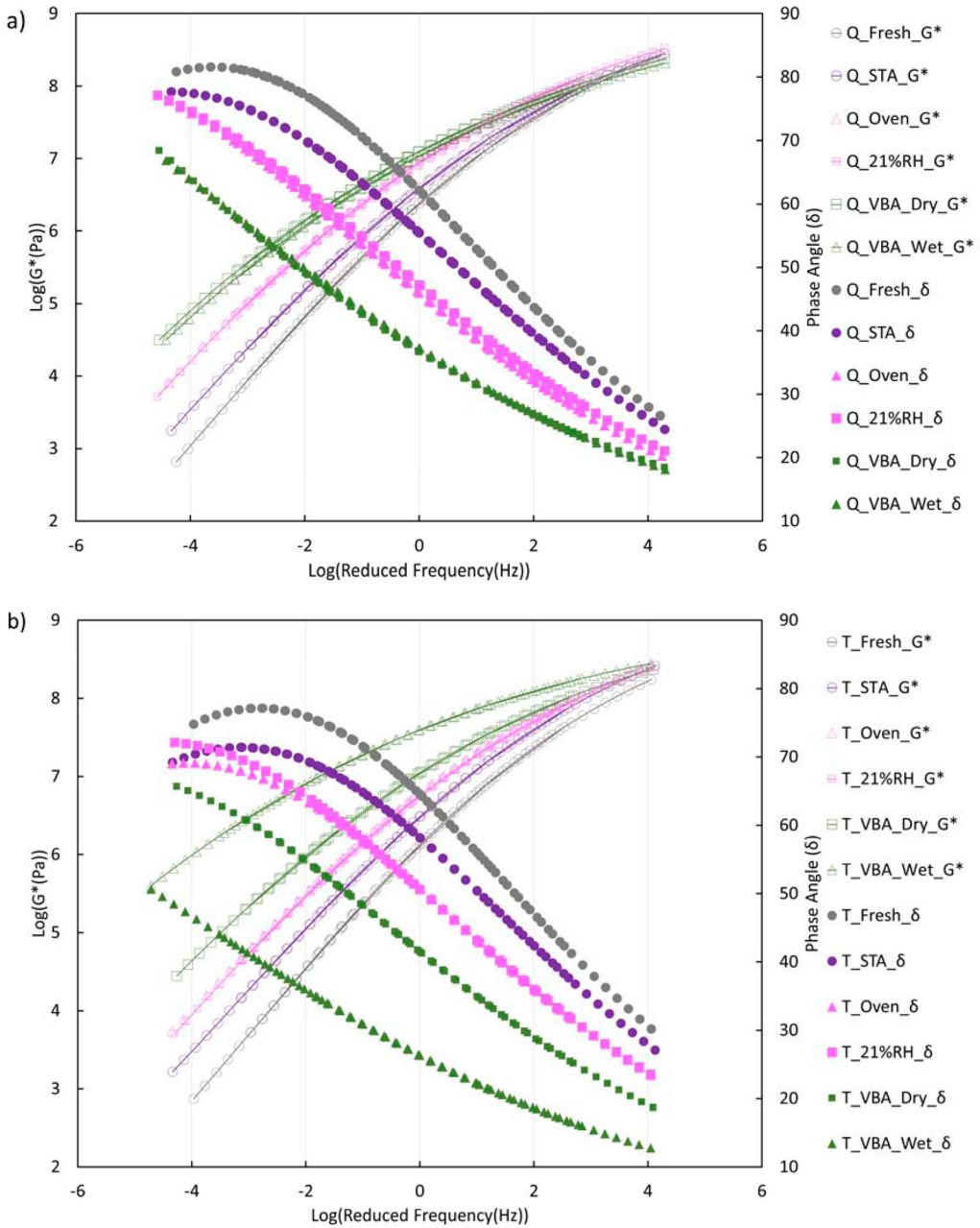


Figure 5. Master curves (at 20°C) of (a) Q binder, and (b) T binder at all aging states, i.e. fresh, TFOT short-term aged, oven aged, humidity aged, VBA-Dry and VBA-Wet.

molecular mass, prolonged relaxation time, and increased softening point. Conversely, reduced CR-CM values suggest a wider range of molecular masses, signifying greater polydispersity (Jing et al., 2020).

Figure 6 illustrates the logarithmic representations of CR-CM for all tested samples plotted against the corresponding logarithmic CR-Fr values for both Q and T bitumen. The aging process resulted in a notable decrease in both CR-CM and CR-Fr. For T binder, oven-aged and humidity-aged samples fall within a comparable range of crossover values, as indicated by the standard deviations. Nevertheless,

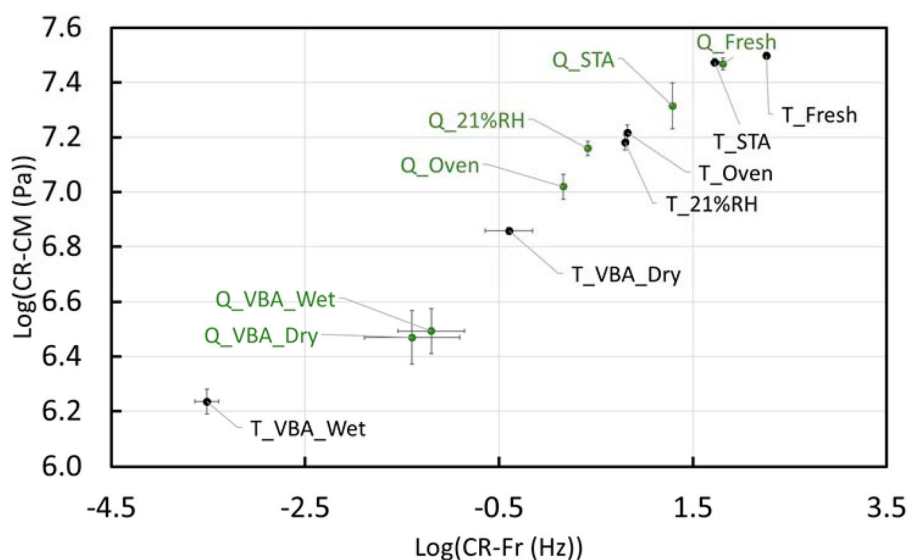


Figure 6. Crossover complex modulus versus crossover frequency of Q and T binders at all aging states, i.e. fresh, TFOT short-term aged, oven aged, humidity aged, VBA-Dry and VBA-Wet.

the oven aging process for the Q sample exhibits lower crossover values, indicative of a more extensively aged sample. This observation aligns with the findings from the phase angle master curves, specifically at high and medium frequencies, where the oven-aged Q sample demonstrates lower values compared to aging solely with humidity. Importantly, the crossover plot provides a more evident illustration of the aging difference than the master curves. Moreover, the wet and dry aged samples of Q binder closely align in the same range of crossover values. T binder displayed significant sensitivity to aging in VBA-Wet condition, with both CR-Fr and CR-CM values of T-VBA-Wet samples being extremely low, indicating substantial aging, in line with FTIR findings.

Relaxation

To comprehensively assess the characteristics of aged samples, Figure 7a illustrates a plot showing the ratio of residual shear stress to initial shear stress. As bitumen undergoes aging, it becomes less viscous and exhibits greater stiffness. Consequently, a more aged sample displays a higher ratio of residual shear stress to initial shear stress, indicating reduced recovery ability (Jing et al., 2021). This reduction in recovery ability is evident after both short-term and long-term aging for both binders. In the case of the Q binder, the ratio experienced a more pronounced increase in oven-aged samples as opposed to those aged solely with humidity. This observation is consistent with the outcomes obtained from both frequency sweep and FTIR analyses. Notably, for the Q binder, the ratio remains equal for VBA-Wet and VBA-Dry samples, signifying a similar degree of aging under these conditions. In contrast, for the T binder, this ratio notably increases for samples aged under VBA-Wet conditions compared to those aged under VBA-Dry conditions, indicating more severe aging with VBA-Wet. This observation aligns with the results from FTIR spectroscopy and frequency sweep tests.

For bitumen to be suitable as a road construction material, it must possess the ability to withstand continuous traffic loads, requiring short relaxation times to prevent stress accumulation in the pavement. Figure 7b presents an analysis of relaxation times for different samples, specifically the time needed for shear stress to decrease to 25% and 50% of the initial stress. Aging leads to an increase in the relaxation time required to reach these stress percentages, with this increase being more significant in long-term aged samples, particularly those subjected to VBA-Wet aging. This phenomenon

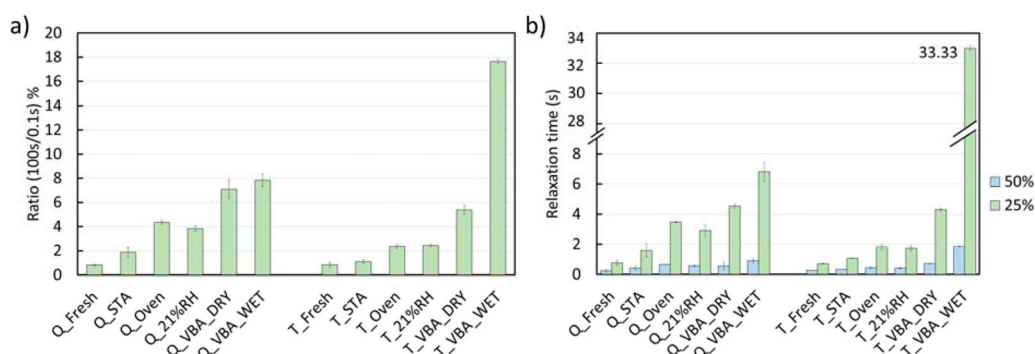


Figure 7. Relaxation results, (a) ratio of residual shear stress (100s) vs the initial shear stress (0.1s), (b) Relaxation time when the shear stress was reduced to 25 and 50% of the initial stress for Q and T binders at all aging states, i.e. fresh, TFOT short-term aged, and VBA-Dry, and VBA-Wet.

is primarily due to the higher viscosity of these aged samples. This evaluation aligns with the FTIR results, where wet-aged samples exhibited higher indices, indicating more aging. It is worth noting that within a single characterisation method, different indices may exhibit varying degrees of sensitivity in revealing the extent of aging in samples. For example, in the case of Q binders, the ratio of residual shear stress to initial shear stress was unable to distinguish between VBA-Wet and VBA-Dry conditions, whereas the time required for shear stress to decrease to 25% and 50% of the initial stress clearly highlighted this difference. In summary, VBA-Wet conditions have a more pronounced impact on the relaxation ability of both binders compared to dry aging, but the extent of this impact depends on the binder type and its sensitivity to VBA-Wet conditioning.

Up to this point, through the utilisation of FTIR, frequency sweep and relaxation tests, we have demonstrated that VBA-Dry and VBA-Wet aging represent the most severe conditions for both binders. Consequently, for the subsequent characterisations in this paper, the focus will solely include the VBA-Dry and VBA-Wet conditions.

SARA fractionation

Figure 8 shows the results of the SARA fractionation analysis for samples Q and T under different aging conditions. The aging process resulted in a decrease in the saturated and aromatic fractions for both binders, indicating the evaporation of volatiles or/and a conversion of these fractions to more polar molecules during aging. Binder Q experienced a smaller decrease than binder T because it has higher oxygen content and consequently lower sensitivity to aging.

The content of highly polar fractions, namely resins and asphaltenes, increased after both short-term and long-term aging. This can be attributed to the oxidation-induced transformation of molecules from saturated and aromatic compounds. Combining fractions containing aromatic rings (aromatics, resins and asphaltenes) shows an increase in content after aging, aligning with the trend exhibited by the aromatic index from the FTIR analysis. Combined aging with reactive oxygen species (ROS) and moisture affected the Q and T samples to varying degrees. Specifically, dry aging with ROS resulted in greater aging of the Q bitumen, while the T bitumen exhibited greater aging under the combined aging conditions. From the comparison of the changes in the content values after the individual aging stages, it can be concluded that the T bitumen is more susceptible to VBA-Wet aging compared to the Q bitumen. The elevated content of asphaltenes in sample T-VBA-Wet may be attributed to the low oxygen content of this binder (Table 1). Binders with higher initial oxygen content may already contain oxygenated functional groups, potentially influencing the reactivity and susceptibility to further oxidation. Conversely, binders with lower oxygen content may undergo more significant changes in their structure when exposed to the reactive products. The strong aging of sample T-VBA-Wet is

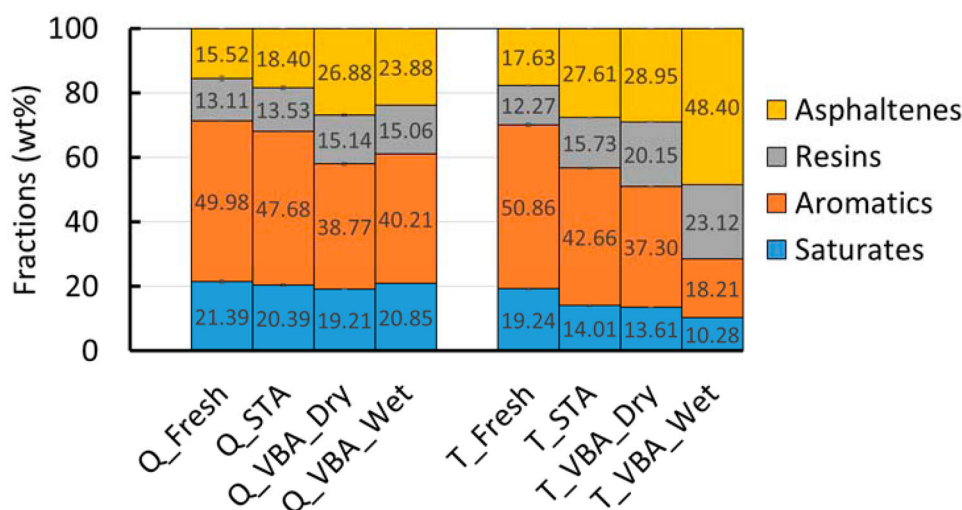


Figure 8. Aging effect on SARA fractions of Q and T bitumen

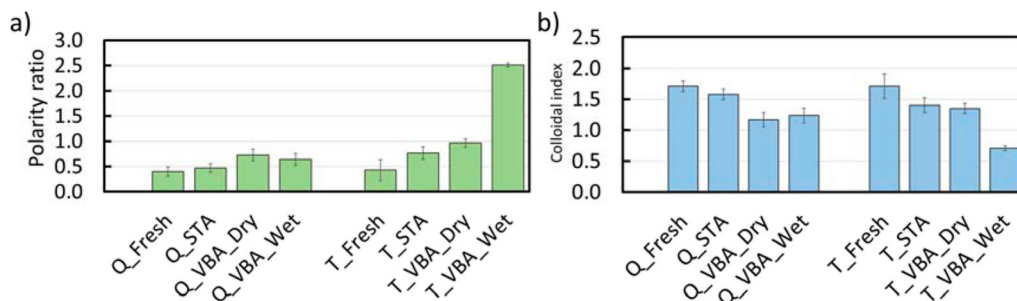


Figure 9. Aging effects on (a) polarity ratio and (b) colloidal index CI of Q and T bitumen.

consistent with the results of FTIR, where this sample showed the highest indices of sulfoxide and carbonyl.

The polarity ratio, i.e. the ratio of highly polar (resin and asphaltenes) to light molecular weight (saturated and aromatic) fractions, is shown in Figure 9a and b. After long-term aging, the polarity ratio of the Q samples increases by 1.8 and 1.6 times for VBA-Dry and VBA-Wet, respectively. As for long-term aging of the T samples, the ratios for VBA-Dry and VBA-Wet increased to 2.2 and 5.8 times, respectively. There is a significant difference between the polarity ratio of the Q and T samples, indicating a difference in aging sensitivity. Long-term aging significantly changes the relative ratio of high/low polarity components, disturbing the original colloidal equilibrium and promoting the agglomeration of high polarity fractions to reduce the surface energy of polar molecules and adapt to the new solvent environment with limited saturated and aromatic fractions (Ren et al., 2022).

Figure 9b illustrates the Colloidal Index (CI) values of fresh and aged binders. According to Ashoori et al. the stability of crude oil can be determined from the CI values, with values above 1.42 indicating stability and values below 1.11 indicating instability (Ashoori et al., 2017). Thus, both fresh and short-term aged samples exhibit stability, while long-term aging leads to instability in the structure of both binders. From a colloid chemistry perspective, the instability of the colloidal structure primarily arises from the imbalance between the micelles (asphaltene and resin) and the dispersion medium (aromatic and saturated). The increase in the number of micelles and the decrease in the dispersion medium both accelerate the micelle aggregation and settling (Ren et al., 2022). It is noteworthy that

the sample T-VBA-Wet has the lowest CI value, indicating the highest degree of instability. In conclusion, the SARA fractionation shows that aging with ROS leads to an increase in the polar fraction of the bitumen components and to the instability of the colloidal structure. In addition, the effect of adding moisture to ROS to increase the degree of aging depends on the sensitivity of bitumen to aging.

Optical inverse bright-, darkfield and fluorescence microscope (OIM)

Bee-like structures in bitumen, first described by Loeber et al. (1996), are wavy, rippled surface patterns observed through microscopy techniques and have been a subject of ongoing debate regarding their origin (Loeber et al., 1996). Bee-like structures in bitumen are thought to be related to asphaltenes, they may be formed by paraffinic wax crystals or induced by doping with linear n-alkanes. Various microscopy techniques, such as brightfield, darkfield and fluorescence optical inverse microscopy (OIM), as well as confocal laser scanning microscopy (CLSM) and atomic force microscopy (AFM), have been employed to investigate bitumen's surface microstructure (Werkovits et al., 2023). These studies reveal that bee structures and their characteristics, such as area coverage and density, can change with aging. Recent research demonstrates a decrease in the number of bee structures and an increase in their size after aging, although the exact mechanisms governing these changes are still under investigation (Mirwald et al., 2022a). Understanding the formation and evolution of bee structures through microscopy provides valuable insights into bitumen's aging behaviour.

Figures 10 and 11 show microscopic images captured using OIM, displaying the structures of Q and T binders. The images depicted on the left represent bright-field images, wherein small dark regions are visible, indicating the presence of bee structures. However, for a clearer view of these structures, one needs to refer to the dark field images. It is important to note that the blurring observed in these images is a result of the instrument's limitations, specifically the Abbe limit and resolution. In addition, each bee structure is surrounded by a different region, usually referred to as the peri-phase (Masson et al., 2006). Figures 10 and 11a–d show the corresponding images of fresh, short-aged, VBA-Dry, and VBA-Wet for Q and T samples, respectively. The number of dark spots in the bright-field images increased with aging for Q binder, while these black spots disappeared for the T-VBA-Wet sample, indicating different aging sensitivity and microstructure of Q and T binders.

Dark-field images are shown in the middle column of Figure 10. Dark field microscopy detects only light scattering objects and clearly shows the bee structure. This confirms that the bee structures have different physical (optical) properties than the rest of the material and become visible in the dark field. Comparing the Q images in Figure 10, the number of bee structures on the surface of the bitumen increased due to short-term and long-term aging. For binder T in Figure 11, sample T-VBA-Wet showed only a few bee structures, while the short term aged, and VBA-Dry aged samples showed an increased number of bee structures as compared to the fresh sample.

Figure 12 illustrates the area percentage of bee structures on the surface of the dark field images. The percentage of the surface area of the Q-aged samples is the same, while the T samples show a significant increase in the surface area covered by bee structures after short- and long-term dry aging. On the other hand, coupled long-term aging with ROS and moisture caused a sharp decrease in the percentage of surface area covered by bee structures. From the FTIR, DSR and SARA fractionation results, it is known that the T-VBA-Wet sample was strongly aged. So, it seems that strongly aged bitumen with unstable microstructure, i.e. polarity ratio more than 1, is not able to form the bee structure on the surface. It is worth noting that some of the samples in Figure 12 have a larger standard deviation, which shows the complexity of the material and the diversity within a sample. Even with adherence to rigorous sample preparation techniques (Mirwald et al., 2022a), significant differences in surface microstructure can be observed.

The fluorescence images are shown in the right column of Figures 10 and 11. Interestingly, the peri-phase around the bee structures shows a higher fluorescence signal than the rest of the sample surface. Since the fluorescence excitation filter used is in the range of 350–450 nm, which corresponds to the fluorescence of compounds with three to four and five or more polyaromatic rings, following

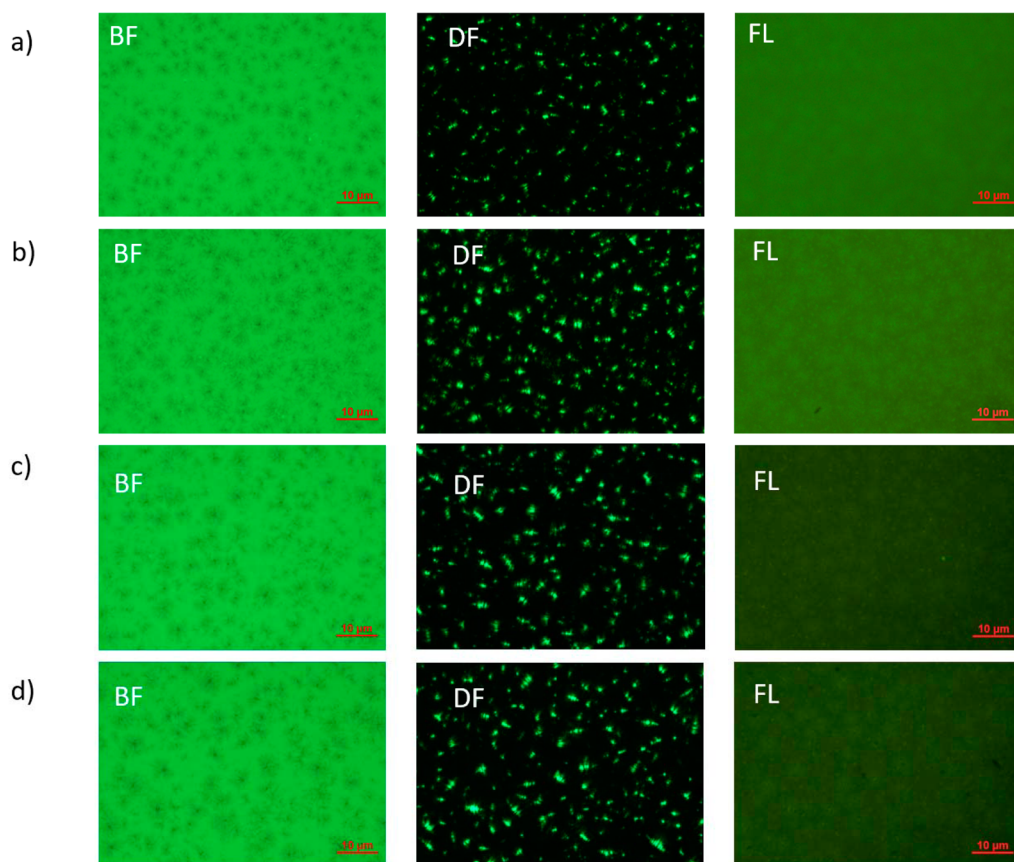


Figure 10. Microscopic images of Q binder in the optical microscope, (a) Fresh, (b) short-term aged, (c) VBA-Dry, (d) VBA-Wet. BF = bright field, DF = dark field, FL = fluorescence.

the literature from the early 1990s by Buisine et al. (Buisine et al., 1993). However, it can be clearly seen here that the bee structure in the centre of the peri phase does not exhibit significant annealing. Only certain particles display increased fluorescence, and this cannot be attributed to the bee structure because they are also present in random areas throughout the material, not just in the centre of observed regions in bright-field or dark-field. There is no clear indication of what these bright fluorescent particles can be associated with. In addition, the overall fluorescence intensity of the images decreased with aging. The lowest fluorescence intensity was obtained for the T-VBA-Wet sample with 18.21% aromatics fraction.

In summary, optical microscopy can be a complementary technique to evaluate the microstructure of bitumen and its stability. However, a clear universal quantification technique is needed to analyse the obtained images. Moreover, further studies are needed to explain all the details of the microscopic images.

Summary and conclusion

This study investigated the aging effects of oven-aging, humidity aging, and ROS with and without moisture on two types of bitumen using FTIR spectroscopy, dynamic shear rheometer, SARA Fractionation and optical microscopy.

The FTIR indices showed an increase in carbonyl, sulfoxide, and aromatic indices, and a decrease in the long chain and aliphatic index with aging. However, further investigations are needed to understand the aging patterns for sulphone and hydroxyl indices. The DSR test revealed that G^*

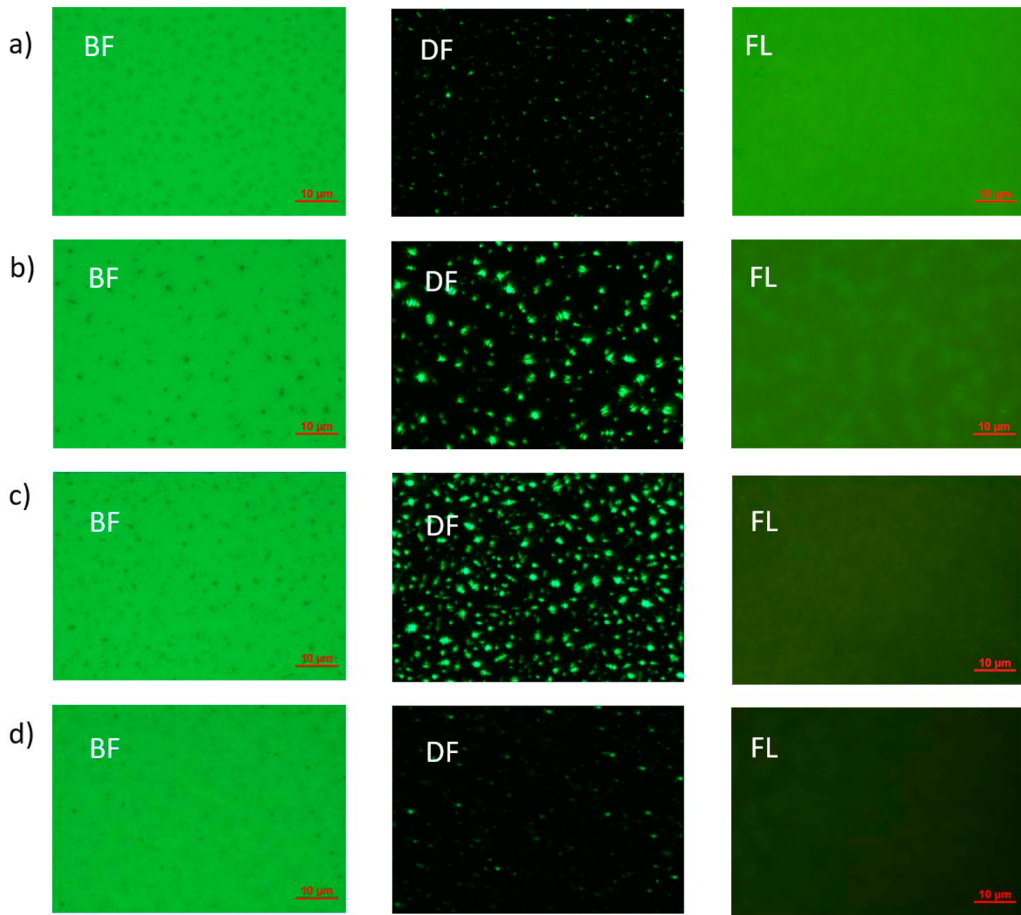


Figure 11. Microscopic images of T binder in the optical microscope, (a) Fresh, (b) short-term aged, (c) VBA-Dry, (d) VBA-Wet. BF = bright field, DF = dark field, FL = fluorescence.

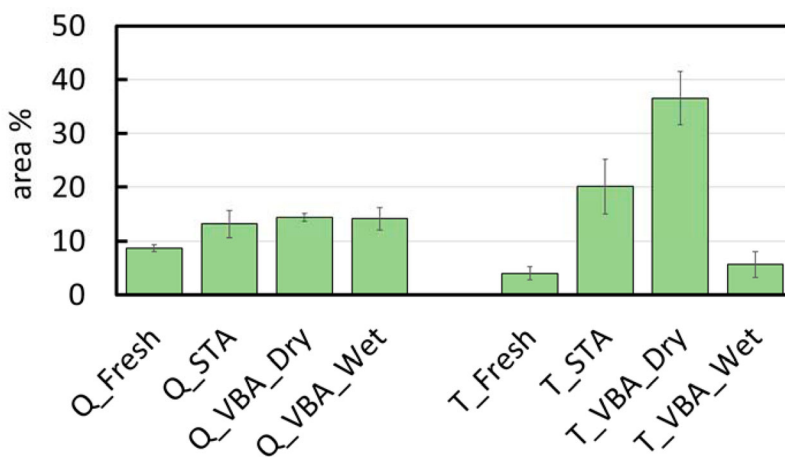


Figure 12. Results from the area covered by bee structure analysis from dark-field (DF)

values increased while the phase angle and crossover values decreased after short-term and long-term aging. For both binders, oven aging exhibited more severe aging compared to aging solely with humidity. Moreover, in the case of Q binder, there was no significant difference between VBA-Wet and VBA-Dry conditions, whereas for T samples, the difference was evident, with VBA-Wet condition causing substantial aging in the T binder. Moreover, the crossover values indicated more aging in Q binder with VBA-Dry, while for T binder, VBA-Wet was the more influential aging condition. According to the relaxation outcomes, it was observed that the VBA-Wet condition has a more pronounced influence on the relaxation properties of both binders in comparison to dry aging. Nonetheless, the extent of this impact varies significantly depending on the binder type and its susceptibility to VBA-Wet conditioning. The analysis revealed that aging led to an increase in asphaltenes and resins, while aromatics and saturates decreased in both short-term and long-term aging, irrespective of the binder type. The severity of aging was influenced by the binder type, with Q bitumen experiencing stronger effects from VBA-Dry aging, while T exhibited more pronounced aging under VBA-Wet conditions. The optical microscopy revealed peri-phase and bee structures on the bitumen surface, with aging leading to more dark spots and an increased surface area covered by bright spots. However, the technique's inability to differentiate between different aging states requires using it as a complementary analysis tool.

In conclusion, the study suggests that the VBA-Wet conditioning could potentially result in more severe aging compared to the VBA-Dry condition, but this difference depends on the specific binder type and its susceptibility to aging. Oven aging and humidity-only aging were also evaluated as control groups, revealing that binders did not exhibit any additional aging when subjected to humidity-only aging. Therefore, additional factors, such as increased reaction of water vapour molecules with ROS, may contribute to enhanced reactive species within the aging chamber, and further research is needed to establish correlations between observed phenomena and the chemical properties of the binders. For future investigations, it is highly recommended to explore higher levels of humidity to examine the influence of humidity concentration and assess the potential interaction between ROS and water vapour molecules. Moreover, analysing each SARA fraction separately enhances the understanding of the process. Exploring more intricate aging methods, such as coupled UV-ROS aging, may be a direction for future research. Furthermore, more advanced, and precise imaging analyses are crucial for optimising the application of microscopy techniques in this context.

Acknowledgments

This paper/article is created under the research programme Knowledge-based Pavement Engineering (KPE). KPE is a cooperation between Rijkswaterstaat, TNO and TU Delft in which scientific and applied knowledge is gained about asphalt pavements and which contributes to the aim of Rijkswaterstaat to be completely climate neutral and to work according to the circular principle by 2030. The opinions expressed in this paper is solely from the authors. The financial support by the Austrian Federal Ministry for Digital and Economic Affairs, the National Foundation for Research, Technology and Development and the Christian Doppler Research Association is gratefully acknowledged. The authors would also like to express their gratitude to the CD laboratory company partners BMI Group, OMV Downstream and Pittel + Brausewetter for their financial support. AV also acknowledges NWO-AES (Dutch Research Council-Applied and Engineering Sciences) for a Talent Programme VENI grant for the project 'A multiscale approach towards future road infrastructure: How to design sustainable paving materials?'

Disclosure statement

No potential conflict of interest was reported by the author(s).

ORCID

Kristina Primerano  <http://orcid.org/0000-0001-5978-1989>

Johannes Mirwald  <http://orcid.org/0000-0001-5025-7427>

Bernhard Hofko  <http://orcid.org/0000-0002-8329-8687>

Aikaterini Varveri  <http://orcid.org/0000-0002-8830-9437>

References

- Airey, G., Collop, A., Zoorob, S., & Elliott, R. (2008). The influence of aggregate, filler and bitumen on asphalt mixture moisture damage. *Construction and Building Materials*, 22(9), 2015–2024. <https://doi.org/10.1016/j.conbuildmat.2007.07.009>
- Airey, G. D. (2003). State of the art report on ageing test methods for bituminous pavement materials. *International Journal of Pavement Engineering*, 4(3), 165–176. <https://doi.org/10.1080/1029843042000198568>
- Ashoori, S., Sharifi, M., Masoumi, M., & Salehi, M. M. (2017). The relationship between SARA fractions and crude oil stability. *Egyptian Journal of Petroleum*, 26(1), 209–213. <https://doi.org/10.1016/j.ejpe.2016.04.002>
- Besamusca, J., Volkers, A., Water, v. d. J., & Gaarkeuken, B. (2012). Simulating ageing of EN 12591 70/100 bitumen at laboratory conditioning compared to porous asphalt. In *5th Eurasphalt and Eurobitume congress*, Istanbul.
- Buisine, J., Joly, G., Eladlani, A., Such, C., Farcas, F., Ramond, G., Claudy, P., Letoffe, J., King, G., & Planche, J. (1993). Thermodynamic behavior and physicochemical analysis of eight SHRP bitumens. *Transportation Research Record* (1386).
- Cong, P., Guo, X., & Ge, W. (2021). Effects of moisture on the bonding performance of asphalt-aggregate system. *Construction and Building Materials*, 295, 123667. <https://doi.org/10.1016/j.conbuildmat.2021.123667>
- Das, P. K., Baaj, H., Kringos, N., & Tighe, S. (2015). Coupling of oxidative ageing and moisture damage in asphalt mixtures. *Road Materials and Pavement Design*, 16(sup1), 265–279. <https://doi.org/10.1080/14680629.2015.1030835>
- EN 12607-1. (2014). C.2014.12607-1: Bitumen and Bituminous Binders—Determination of the Resistance to Hardening under Influence of Heat and Air—Part 1: RTFOT Method. European Committee for Standardization.
- EN 12607-2. (2014). C.2014.12607-1: Bitumen and Bituminous Binders—Determination of the Resistance to Hardening under Influence of Heat and Air—Part 1: RTFOT Method. European Committee for Standardization.
- EN 14769. (2012). C.2012.14769: Bitumen and Bituminous Binders—Accelerated Long-Term Ageing Conditioning by a Pressure Ageing Vessel (PAV). European Committee for Standardization.
- Erskine, J., Hesp, S., & Kaveh, F. (2012). Another look at accelerated aging of asphalt cements in the pressure aging vessel. In *Proceedings, fifth Eurasphalt and Eurobitumen congress, Istanbul, Turkey*.
- Hofer, K., Mirwald, J., Maschauer, D., Grothe, H., & Hofko, B. (2022). Influence of selected reactive oxygen species on the long-term aging of bitumen. *Materials and Structures*, 55(5), 133. <https://doi.org/10.1617/s11527-022-01981-1>
- Hofer, K., Werkovits, S., Schönauer, P., Mirwald, J., Grothe, H., & Hofko, B. (2023). Chemical and mechanical analysis of field and laboratory aged bitumen. *Road Materials and Pavement Design*, 24(sup1), 160–175. <https://doi.org/10.1080/14680629.2023.2180297>
- Hofko, B., & Hospodka, M. (2016). Rolling thin film oven test and pressure aging vessel conditioning parameters: Effect on viscoelastic behavior and binder performance grade. *Transportation Research Record*, 2574(1), 111–116. <https://doi.org/10.3141/2574-12>
- Hofko, B., Maschauer, D., Steiner, D., Mirwald, J., & Grothe, H. (2020). Bitumen ageing – Impact of reactive oxygen species. *Case Studies in Construction Materials*, 13, e00390. <https://doi.org/10.1016/j.cscm.2020.e00390>
- Huang, S.-C., Turner, T., & Thomas, K. (2008). The influence of moisture on the aging characteristics of bitumen. In *Proceedings of the 4th Eurasphalt and Eurobitume Congress held May 2008, Copenhagen, Denmark*.
- Jacob, D. J. (2000). Heterogeneous chemistry and tropospheric ozone. *Atmospheric Environment*, 34(12-14), 2131–2159. [https://doi.org/10.1016/S1352-2310\(99\)00462-8](https://doi.org/10.1016/S1352-2310(99)00462-8)
- Jing, R., Varveri, A., Liu, X., Scarpas, A., & Erkens, S. (2019). Laboratory and field aging effect on bitumen chemistry and rheology in porous asphalt mixture. *Transportation Research Record*, 2673(3), 365–374. <https://doi.org/10.1177/0361198119833362>
- Jing, R., Varveri, A., Liu, X., Scarpas, A., & Erkens, S. (2020). Rheological, fatigue and relaxation properties of aged bitumen. *International journal of pavement engineering*, 21(8), 1024–1033. <https://doi.org/10.1080/10298436.2019.1654609>
- Jing, R., Varveri, A., Liu, X., Scarpas, A., & Erkens, S. (2021). Differences in the ageing behavior of asphalt pavements with porous and stone mastic asphalt mixtures. *Transportation Research Record*, 2675(12), 1138–1149. <https://doi.org/10.1177/03611981211032218>
- Jing, R., Varveri, A., Liu, X., Scarpas, A., & Erkens, S. (2022). Ageing behavior of porous and dense asphalt mixtures in the field. In *Proceedings of the RILEM international symposium on bituminous materials: ISBM Lyon 2020 1*, Springer.
- Jing, R., Varveri, A., Liu, X., Scarpas, T., & Erkens, S. (2018). Chemo-mechanics of ageing on bituminous materials. In *97th Annual meeting of the transportation research board, Washington, DC*.
- Khalighi, S., Erkens, S., & Varveri, A. (2024). Exploring the impact of humidity and water on bituminous binder aging: a multi-variate analysis approach (TI CAB). *Road Materials and Pavement Design*, 1–25. <https://doi.org/10.1080/14680629.2024.2364189>
- Koyun, A., Büchner, J., Wistuba, M. P., & Grothe, H. (2022). Rheological, spectroscopic and microscopic assessment of asphalt binder ageing. *Road Materials and Pavement Design*, 23(1), 80–97. <https://doi.org/10.1080/14680629.2020.1820891>
- Loeber, L., Sutton, O., Morel, J., Valletton, J.-M., & Muller, G. (1996). New direct observations of asphalts and asphalt binders by scanning electron microscopy and atomic force microscopy. *Journal of Microscopy*, 182(1), 32–39. <http://doi.org/10.1046/j.1365-2818.1996.134416.x>

- López-Montero, T., & Miró, R. (2016). Differences in cracking resistance of asphalt mixtures due to ageing and moisture damage. *Construction and Building Materials*, 112, 299–306. <https://doi.org/10.1016/j.conbuildmat.2016.02.199>
- Lu, X., Talon, Y., & Redelius, P. (2008). 406-001 Aging of bituminous binders–Laboratory tests and field data. In *4th Eurasphalt Eurobitume congress*.
- Ma, L., Salehi, H. S., Jing, R., Erkens, S., Vlugt, T. J., Moulto, O. A., Greenfield, M. L., & Varveri, A. (2023). Water diffusion mechanisms in bitumen studied through molecular dynamics simulations. *Construction and Building Materials*, 409, 133828. <https://doi.org/10.1016/j.conbuildmat.2023.133828>
- Masson, J. F., Leblond, V., & Margeson, J. (2006). Bitumen morphologies by phase-detection atomic force microscopy. *Journal of microscopy*, 221(1), 17–29. <https://doi.org/10.1111/j.1365-2818.2006.01540.x>
- Mirwald, J., Hofko, B., Pipintakos, G., Blom, J., & Soenen, H. (2022a). Comparison of microscopic techniques to study the diversity of the bitumen microstructure. *Micron*, 159, 103294. <https://doi.org/10.1016/j.micron.2022.103294>
- Mirwald, J., Maschauer, D., Hofko, B., & Grothe, H. (2020a). Impact of reactive oxygen species on bitumen aging–The Vienne binder aging method. *Construction and Building Materials*, 257, 119495. <https://doi.org/10.1016/j.conbuildmat.2020.119495>
- Mirwald, J., Nura, D., Eberhardsteiner, L., & Hofko, B. (2022b). Impact of UV–Vis light on the oxidation of bitumen in correlation to solar spectral irradiance data. *Construction and Building Materials*, 316, 125816. <https://doi.org/10.1016/j.conbuildmat.2021.125816>
- Mirwald, J., Werkovits, S., Camargo, I., Maschauer, D., Hofko, B., & Grothe, H. (2020b). Understanding bitumen ageing by investigation of its polarity fractions. *Construction and Building Materials*, 250, 118809. <https://doi.org/10.1016/j.conbuildmat.2020.118809>
- Nagabhushanarao, S. S., & Vijayakumar, A. (2021). Chemical and rheological characteristics of accelerate aged asphalt binders using rolling thin film oven. *Construction and Building Materials*, 272, 121995. <https://doi.org/10.1016/j.conbuildmat.2020.121995>
- Omar, H. A., Yusoff, N. I. M., Mubarak, M., & Ceylan, H. (2020). Effects of moisture damage on asphalt mixtures. *Journal of Traffic and Transportation Engineering (English Edition)*, 7(5), 600–628. <https://doi.org/10.1016/j.jtte.2020.07.001>
- Petersen, J. C. (2009). A review of the fundamentals of asphalt oxidation: chemical, physicochemical, physical property, and durability relationships. Transportation research circular (E-C140).
- Pipintakos, G., Soenen, H., Ching, H. V., Velde, C. V., Van Doorslaer, S., Lemièr, F., & Varveri, A. (2021). Exploring the oxidative mechanisms of bitumen after laboratory short-and long-term ageing. *Construction and Building Materials*, 289, 123182. <https://doi.org/10.1016/j.conbuildmat.2021.123182>
- Qian, Y., Guo, F., Leng, Z., Zhang, Y., & Yu, H. (2020). Simulation of the field aging of asphalt binders in different reclaimed asphalt pavement (RAP) materials in Hong Kong through laboratory tests. *Construction and Building Materials*, 265, 120651. <https://doi.org/10.1016/j.conbuildmat.2020.120651>
- Qin, Q., Schabron, J. F., Boysen, R. B., & Farrar, M. J. (2014). Field aging effect on chemistry and rheology of asphalt binders and rheological predictions for field aging. *Fuel*, 121, 86–94. <https://doi.org/10.1016/j.fuel.2013.12.040>
- Read, J., & Whiteoak, D. (2003). *The shell bitumen handbook*. Thomas Telford.
- Ren, S., Liu, X., Lin, P., Jing, R., & Erkens, S. (2022). Toward the long-term aging influence and novel reaction kinetics models of bitumen. *International Journal of Pavement Engineering*, 24(2), 1–16.
- Sakib, N., & Bhasin, A. (2019). Measuring polarity-based distributions (SARA) of bitumen using simplified chromatographic techniques. *International Journal of Pavement Engineering*, 20(12), 1371–1384. <https://doi.org/10.1080/10298436.2018.1428972>
- Singh, C. V., Pachauri, P., Dwivedi, S. P., Sharma, S., & Singari, R. (2022). Formation of functionally graded hybrid composite materials with Al₂O₃ and RHA reinforcements using friction stir process. *Australian Journal of Mechanical Engineering*, 20(1), 141–154. <https://doi.org/10.1080/14484846.2019.1679583>
- Singhvi, P., Mainieri, J. J. G., Ozer, H., Sharma, B. K., Al-Qadi, I. L., & Morse, K. L. (2022). Impacts of field and laboratory long-term aging on asphalt binders. *Transportation Research Record*, 2676(8), 336–353. <https://doi.org/10.1177/0361198121083614>
- T315. (2012). *A.2012.Standard method of test for determining the rheological properties of asphalt binder using a dynamic shear rheometer (DSR)*. American Association of State Highway and Transportation Officials.
- Valentin, J., Trejbal, J., Nežerka, V., Valentová, T., Vacková, P., & Tichá, P. (2021). A comprehensive study on adhesion between modified bituminous binders and mineral aggregates. *Construction and Building Materials*, 305, 124686. <https://doi.org/10.1016/j.conbuildmat.2021.124686>
- Valentová, T., Altman, J., & Valentin, J. (2016). Impact of asphalt ageing on the activity of adhesion promoters and the moisture susceptibility. *Transportation Research Procedia*, 14, 768–777. <https://doi.org/10.1016/j.trpro.2016.05.066>
- Varveri, A. K. (2017). *Moisture damage susceptibility of asphalt mixtures: Experimental characterization and modelling*.
- Werkovits, S., Bacher, M., Mirwald, J., Theiner, J., Rosenau, T., Hofko, B., & Grothe, H. (2023). The impact of field ageing on molecular structure and chemistry of bitumen. *Fuel*, 343, 127904. <https://doi.org/10.1016/j.fuel.2023.127904>
- Zou, Y., Amirkhanian, S., Xu, S., Li, Y., Wang, Y., & Zhang, J. (2021). Effect of different aqueous solutions on physicochemical properties of asphalt binder. *Construction and Building Materials*, 286, 122810. <https://doi.org/10.1016/j.conbuildmat.2021.122810>